IEEE Access
Multidisciplinary | Rapid Review | Open Access Journal

Received July 26, 2018, accepted August 25, 2018, date of publication September 3, 2018, date of current version October 8, 2018.

Digital Object Identifier 10.1109/ACCESS.2018.2868074

Anti-Disturbance Backstepping Attitude Control for Rigid-Flexible Coupling Spacecraft

YUE MIAO, FENG WANG, AND MING LIU
School of Astronautics, Harbin Institute of Technology, Harbin 150080, China

Corresponding author: Ming Liu (mingliu23@hit.edu.cn)

This work was supported in part by the National Natural Science Foundation of China under Grant 91438202, Grant 61833009, Grant 61473096, Grant 61690212, and Grant 61333003 and in part by the Natural Science Foundation of Heilongjiang Province of China under Grant QC2012C082.

ABSTRACT This paper investigates the problem of attitude stabilization for rigid-flexible coupling spacecraft under external disturbances, parametric uncertainties, and measurement errors. First, the dynamical model for a rigid spacecraft with two symmetric solar arrays is derived based on the Lagrange method, and the measured kinematic and dynamic models are formulated, respectively, in terms of the measured values and errors. A robust anti-disturbance control law is hierarchically proposed to stabilize the attitude states via the backstepping method. For the first step, the lumped disturbance in the measured kinematic model is reconstructed from a finite-time integral sliding mode disturbance observer (FTISMDO), and a virtual control strategy is designed. For the second step, the overall uncertainties in the measured dynamic model are approximated by FTISMDO, and the actual control scheme is proposed based on the virtual control and disturbance observers. It is proved that the designed controller can guarantee that all attitude variables converge to small neighborhoods of origin asymptotically in the presence of interior and exterior disturbances. Finally, a numerical example is provided to demonstrate the disturbance rejection and robustness performance of the proposed control technique.

INDEX TERMS Spacecraft attitude control, baskstepping method, sliding mode disturbance observer, rigid-flexible coupling spacecraft.

I. INTRODUCTION

Space science technology has achieved tremendous advancement in recent years [1]. Complicated aerospace missions, such as space rendezvous and docking [2], [3], deep space exploration [4], spacecraft formation flying [5] and so on, are being widely investigated and practiced in aerospace engineering. Most modern space tasks require accurate pointing and fast stabilization of the spacecraft, thus the attitude control remains a crucial topic [6].

The design of a high-performance attitude controller for a spacecraft is difficult due to the model non-linearities, parametric uncertainties, measurement errors, and unknown external disturbances in space [7]. In addition, spacecrafts may carry large-scale, low stiffness and light weight appendages, such as large deployable antenna and solar arrays, these structures decrease the rigidity of the spacecrafts and result in flexible phenomenon [8]. Especially, the attitude maneuver of the spacecraft platform will unavoidably excite the elastic oscillations of flexible appendages, and the vibration will affect the rotation of the spacecraft via hinges simultaneously, which further results in the decrease of the attitude pointing accuracy [9]. Therefore, it is necessary to take the flexible appendages into account and compensate the adverse effects of the rigid-flexible coupling phenomenon in spacecraft attitude controller design. The vibration items of the flexible appendages can be substituted into the attitude dynamic model via the coupling equation and considered as uncertainties. Then, external disturbance, measurement errors, and model uncertainties are lumped as total disturbance. Quite often, the lumped disturbance cannot be directly measured, which however must be properly considered in the spacecraft attitude controller design. Moreover, these uncertainties can lead to inaccurate pointing of the spacecraft payload, or even the instability of the spacecraft platform. For solving this problem, a feasible way is to estimate the lumped uncertainties by the disturbance observer technique [10].

The state and disturbance observer technique has been extensively studied for nearly half a century, and a variety of observers, like disturbance observer [11], perturbation observer [12], extended state observer [13], unknown input

observer [14], etc [15], have been employed to deal with the estimation problems for various types of dynamical system, such as uncertain linear/nonlinear systems [16], [17], discrete-time systems [18]–[20], Markovian jump systems [21], hybrid systems [22], singular systems [23], switched systems [24], [25], etc [15], [26]. Since the sliding mode control stands out for its strong robustness against system uncertainties and external disturbance, sliding mode observers have also been widely researched for system state and disturbance estimations [27]. For example, Liu et al. [28] designed a proportional and derivative sliding mode observer to generate the asymptotic estimation for system states and sensor fault vectors of Markovian jump systems, Zhang et al. [29] proposed a sliding mode friction observer to estimate the reaction wheel friction torque for flexible spacecraft, Chen et al. [30] developed a terminal sliding mode disturbance observer to compensate the unknown external disturbance for the single-input and single-output nonlinear system, etc. Sun et al. [31] constructed a finite-time integral sliding mode observer to evaluate the external disturbance and appendage vibration of the flexible spacecraft. It has proved that the proposed observer can effectively estimate the lumped uncertainties in finite time. The integral operation in sliding mode observer can remarkably increase the convergence performance and attenuate the chattering effect.

The idea of the disturbance-observer-based control is to evaluate the uncertainties from measurable variables, then design the control scheme based on the estimation, in order to compensate the influence of the disturbances. When the flexible appendages are included in the dynamic model, the attitude controller design becomes more complex due to the complicated nonlinear dynamics [41]. The disturbance-observer-based control for flexible spacecraft has drawn lots of attention, and various nonlinear attitude control methods, such as optimal control [32], the Lyapunov control [33], [34], sliding mode control [35], adaptive control [36], [37], back stepping control [38], [39], etc, are utilized to synthesis work of attitude control systems. Ma [36] developed a fault-tolerant adaptive controller for attitude tracking of flexible spacecraft, Ding and Zheng [40] investigated a non-smooth attitude-stabilization controller based on the finite time control technique, Wu and Wen [41] applied the robust H_∞ output feedback control to achieve attitude stabilization of a flexible spacecraft. Sun et al. [31] proposed a composite anti-disturbance controller via backstepping method, while the control torque needed is relatively high for the actual engineering. Zhang et al. [29] designed a H_∞ controller with disturbance observers for the flexible spacecraft, the inertia uncertainties and measurement errors are not taken into consideration, Du and Li [42] derived a distributed delayed attitude controller by combining the backstepping method with the finite-time control technique for a group of flexible spacecrafts. In this design, communication delays are considered, while parametric and measurement uncertainties are not included. From the brief survey mentioned above, considerable progress has been made in the field of disturbance-observer-based control for flexible spacecraft attitude control. However, there exist some potential problems: 1) the sensors measurement errors and model parametric uncertainties are not being considered in the disturbance models; 2) controller with excellent robustness performance may require large size control torque which is difficult to be implemented by the onboard actuator due to amplitude limitation.

Motivated by aforementioned analysis, a FTISMDO-based backstepping controller with input constraint is designed in this paper. The main contributions are listed as follows: 1) the attitude dynamic model for a rigid satellite with two symmetric solar arrays are provided via the Lagrange method; 2) the external disturbance in space, spacecraft parametric uncertainties, attitude sensor measurement errors, and vibration of flexible appendages are conducted as lumped disturbances and compensated by FTISMDOs; 3) the measured attitude, angular velocity and the modal coordinate of flexible appendages converge to origin aymptotically under the designed controller, and the corresponding actual controlled states converge to small neighborhoods of origin in the presence of measurement errors.

The rest of the paper is organized as follows: the problem formulation is presented in Section II; design process for the anti-disturbance controller is presented in Section III, followed by numerical example and conclusion in Section IV and Section V respectively.

II. PROBLEM FORMULATION

A rigid satellite with two symmetric flexible solar arrays is considered in this paper. The mathematic model for the rigid-flexible coupling spacecraft can be depicted by the kinematic and dynamic equations as follows.

A. THE KINEMATIC EQUATION

To avoid singularities in the parameter, the four unitary quaternion $\boldsymbol{q} \in \mathbb{R}^4$ is employed to describe the attitude of the satellite, and it has the expression:

$$\boldsymbol{q} = \begin{bmatrix} q_0 & \boldsymbol{q}_v^{\mathrm{T}} \end{bmatrix}^{\mathrm{T}} = \begin{bmatrix} q_0 & q_1 & q_2 & q_3 \end{bmatrix}^{\mathrm{T}} \tag{1}$$

where q_0 is the scalar part and $\boldsymbol{q}_v \in \mathbb{R}^3$ is the vector part, and they satisfy $q_0^2 + \boldsymbol{q}_v^{\mathrm{T}}\boldsymbol{q}_v = 1$. The kinematic equation in terms of the quaternion takes the form:

$$\dot{\boldsymbol{q}} = E(\boldsymbol{q})\,\boldsymbol{\omega} = \frac{1}{2}\begin{bmatrix} -\boldsymbol{q}_v^{\mathrm{T}} \\ \tilde{\boldsymbol{q}}_v + q_0 \boldsymbol{I}_{3\times 3} \end{bmatrix} * \boldsymbol{\omega} \tag{2}$$

where $\boldsymbol{\omega} \in \mathbb{R}^3$ is the angular velocity of the undeformed satellite in the body-fixed reference frame $\Re_B$, and $\tilde{\boldsymbol{q}}_v \in \mathbb{R}^{3\times 3}$ represents the skew symmetric matrix of $\boldsymbol{q}_v$.

The relationships for the satellite attitude in three frame, that is, the Earth-centered inertial reference frame $\Re_J$, the orbit reference frame $\Re_O$, and $\Re_B$, can be illustrated in Fig. 1.

As been shown in Fig.1, $\boldsymbol{q}(\boldsymbol{\omega})/\boldsymbol{q}_e(\boldsymbol{\omega}_e)/\boldsymbol{q}_d(\boldsymbol{\omega}_d)$ is the attitude (attitude velocitiy) orientation in $\Re_B/\Re_B/\Re_O$ with respect to $\Re_J/\Re_O/\Re_J$ respectively. $\boldsymbol{q}_e$ is defined as the error

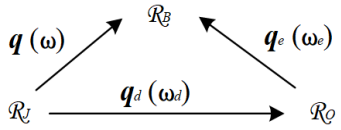

FIGURE 1. Attitudes in the three frames.

quaternion, the error kinematic equation in terms of $\boldsymbol{q}_e$ is formulated as:

$$\boldsymbol{q}_e = E\left(\boldsymbol{q}_e\right)\boldsymbol{\omega}_e = \boldsymbol{E}\left(\boldsymbol{q}_e\right)\left(\boldsymbol{\omega} - \boldsymbol{R}\left(\boldsymbol{q}_e\right)\boldsymbol{\omega}_d\right) \tag{3}$$

where $\boldsymbol{R}\left(\boldsymbol{q}_e\right)$ is the coordinate transformation matrix from $\Re_O$ to $\Re_B$. Since the orbit velocity $\boldsymbol{\omega}_d$ indicates slow motion compared with the attitude manuver $\boldsymbol{\omega}$, it is not considered for simplification in this paper. Therefore, the error kinematic equation is rewritten as:

$$\boldsymbol{q}_e = \boldsymbol{E}\left(\boldsymbol{q}_e\right)\boldsymbol{\omega} \tag{4}$$

B. THE DYNAMIC EQUATION

A rigid satellite with two symmetric flexible solar arrays is illustrated in Fig.2.

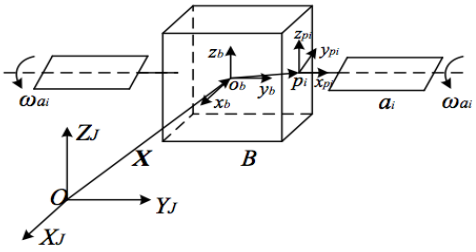

FIGURE 2. A rigid spacecraft with two symmetric flexible appendages.

In Fig.2, $a_i\,(i = 1, 2)$ represents each of the two solar arrays. To be simplified, the satellite translation ($\boldsymbol{X}$ in Fig.2) and the a_i's rotation relative to the satellite ($\boldsymbol{\omega}_{a_i}$ in Fig.2) are not taken into consideration in this paper. Then, according to the Lagrange method [43], the attitude dynamic equation can be described as:

$$\begin{aligned} &\boldsymbol{I}_s\dot{\boldsymbol{\omega}} + \tilde{\boldsymbol{\omega}}\boldsymbol{I}_s\boldsymbol{\omega} + \sum_{i=1}^{2}\boldsymbol{F}_{sa_i}\ddot{\boldsymbol{\eta}}_{a_i} = \boldsymbol{u} + \boldsymbol{d} \\ &\ddot{\boldsymbol{\eta}}_{a_i} + 2\boldsymbol{\xi}_{a_i}\boldsymbol{\Omega}_{a_i}\dot{\boldsymbol{\eta}}_{a_i} + \boldsymbol{\Lambda}_{a_i}\boldsymbol{\eta}_{a_i} + \boldsymbol{F}_{sa_i}^{\mathrm{T}}\dot{\boldsymbol{\omega}} = 0 \end{aligned} \tag{5}$$

where $\boldsymbol{I}_s \in \mathbb{R}^{3\times3}$ is the spacecraft inertial matrix, $\boldsymbol{\eta}_{a_i} \in \mathbb{R}^{N\times1}$ is the modal coordinates of a_i, and N is the number of flexible modes, $\boldsymbol{F}_{sa_i} \in \mathbb{R}^{3\times N}$ is the flexible coupling coefficient matrix of the a_i's vibration to the platform's rotation. $\boldsymbol{u} \in \mathbb{R}^3$ is the control torque, $\boldsymbol{d} \in \mathbb{R}^3$ is the external disturbance. $\boldsymbol{\Omega}_{a_i} \in \mathbb{R}^{N\times N}$ is the modal frequency diagonal matrix, $\boldsymbol{\Lambda}_{a_i} \in \mathbb{R}^{N\times N}$ is the stiffness matrix, and satisfies $\boldsymbol{\Omega}_{a_i}{}^2 = \boldsymbol{\Lambda}_{a_i}$. $\boldsymbol{\xi}_{a_i} \in \mathbb{R}^{N\times N}$ is the damping ratio diagonal matrix. Since the two solar arrays are installed symmetrically, the following equations hold: $\boldsymbol{F}_{sa_1} = \boldsymbol{F}_{sa_2}$, $\boldsymbol{\Lambda}_{a_1} = \boldsymbol{\Lambda}_{a_2}$ and $\boldsymbol{\xi}_{a_1} = \boldsymbol{\xi}_{a_2}$. Therefore, $\boldsymbol{F}_{sa}$, $\boldsymbol{\Lambda}_a$ and $\boldsymbol{\xi}_a$ are utilized to represent $\boldsymbol{F}_{sa_i}$, $\boldsymbol{\Lambda}_{a_i}$ and $\boldsymbol{\xi}_{a_i}$ respectively in the following discussion.

C. THE MEASURED MODELS

The uncertainties considered in this paper include: the measurement error of the attitude sensors onboard the spacecraft, which are expressed as $\Delta\boldsymbol{q}_e$ and $\Delta\boldsymbol{\omega}$ respectively, the unknown external disturbance $\boldsymbol{d}$, and uncertainties of the spacecraft inertial matrix $\Delta\boldsymbol{I}_s$.

Assumption 1: Assume that all the aforementioned uncertainties are bounded: $\|\Delta\boldsymbol{q}_e\| \le \Delta\bar{\boldsymbol{q}}_e$, $\|\Delta\boldsymbol{\omega}\| \le \Delta\bar{\boldsymbol{\omega}}$, $\|\boldsymbol{d}\| \le \bar{\boldsymbol{d}}$, $\|\Delta\boldsymbol{I}_s\| \le \Delta\bar{\boldsymbol{I}}_s$. Moreover, their derivatives are also bounded such that: $\|\Delta\dot{\boldsymbol{q}}_e\| \le \Delta\dot{\bar{\boldsymbol{q}}}_e$, $\|\Delta\dot{\boldsymbol{\omega}}\| \le \Delta\dot{\bar{\boldsymbol{\omega}}}$, $\|\dot{\boldsymbol{d}}\| \le \dot{\bar{\boldsymbol{d}}}$, $\|\Delta\dot{\boldsymbol{I}}_s\| \le \Delta\dot{\bar{\boldsymbol{I}}}_s$. All the bounds are pre-known positive parameters.

Set $\hat{\boldsymbol{q}}_e$ and $\hat{\boldsymbol{\omega}}_s$ as the measured quaternion and attitude velocity respectively, and they are denoted by:

$$\begin{aligned} \hat{\boldsymbol{q}}_e &= \boldsymbol{q}_e + \Delta\boldsymbol{q}_e \\ \hat{\boldsymbol{\omega}} &= \boldsymbol{\omega} + \Delta\boldsymbol{\omega} \end{aligned} \tag{6}$$

where $\boldsymbol{q}_e$ and $\boldsymbol{\omega}$ indicate the actual attitude parameters. For the actual inertial matrix $\boldsymbol{I}_s$, it satisfies:

$$\boldsymbol{I}_s = \hat{\boldsymbol{I}}_s + \Delta\boldsymbol{I}_s \tag{7}$$

where $\hat{\boldsymbol{I}}_s$ is the nominal inertial matrix. Based on formula (4) and (6), the kinematic equation can be expressed as:

$$\dot{\hat{\boldsymbol{q}}}_e - \Delta\dot{\boldsymbol{q}}_e = E\left(\hat{\boldsymbol{q}}_e - \Delta\boldsymbol{q}_e\right)\left(\hat{\boldsymbol{\omega}} - \Delta\boldsymbol{\omega}\right) \tag{8}$$

Further, the measured kinematic equation can be presented as:

$$\dot{\hat{\boldsymbol{q}}}_e = E\left(\hat{\boldsymbol{q}}_e\right)\hat{\boldsymbol{\omega}} + \boldsymbol{\delta}_1 \tag{9}$$

where $\boldsymbol{\delta}_1$ is the lumped uncertainties, and it contains:

$$\boldsymbol{\delta}_1 = -E\left(\hat{\boldsymbol{q}}_e\right)\Delta\boldsymbol{\omega} - E\left(\Delta\boldsymbol{q}_e\right)\boldsymbol{\omega} + \Delta\boldsymbol{q}_e \tag{10}$$

For the rigid-flexible coupling dynamics (5), the two sub-equations can be combined as:

$$\boldsymbol{J}\dot{\boldsymbol{\omega}} + \tilde{\boldsymbol{\omega}}\boldsymbol{I}_s\boldsymbol{\omega} + 2\boldsymbol{F}_{sa}\left(-2\boldsymbol{\xi}_a\boldsymbol{\Omega}_a\dot{\boldsymbol{\eta}}_a - \boldsymbol{\Lambda}_a\boldsymbol{\eta}_a\right) = \boldsymbol{u} + \boldsymbol{d} \tag{11}$$

where $\boldsymbol{J} = \left(\boldsymbol{I}_s - 2\boldsymbol{F}_{sa}\boldsymbol{F}_{sa}^{\mathrm{T}}\right)$. Similarly, considering the uncertainties, formula (11) can be transformed into the measured dynamic equation:

$$\hat{\boldsymbol{J}}\dot{\hat{\boldsymbol{\omega}}} + \hat{\boldsymbol{\omega}}\hat{\boldsymbol{I}}_s\hat{\boldsymbol{\omega}} = \boldsymbol{\delta}_2 + \boldsymbol{u} \tag{12}$$

where $\hat{\boldsymbol{J}} = \left(\hat{\boldsymbol{I}}_s - 2\boldsymbol{F}_{sa}\boldsymbol{F}_{sa}^{\mathrm{T}}\right)$, and $\boldsymbol{\delta}_2$ is the lumped uncertainties which can be expressed as:

$$\begin{aligned} \boldsymbol{\delta}_2 = \boldsymbol{d} &+ 4\boldsymbol{F}_{sa}\boldsymbol{\xi}_a\boldsymbol{\Omega}_a\dot{\boldsymbol{\eta}}_a + 2\boldsymbol{F}_{sa}\boldsymbol{\Lambda}_a\boldsymbol{\eta}_a + \hat{\boldsymbol{J}}\Delta\dot{\boldsymbol{\omega}} - \Delta\boldsymbol{I}_s\dot{\boldsymbol{\omega}} \\ &+ \tilde{\hat{\boldsymbol{\omega}}}\hat{\boldsymbol{I}}_s\Delta\boldsymbol{\omega} - \tilde{\hat{\boldsymbol{\omega}}}\Delta\boldsymbol{I}_s\boldsymbol{\omega} + \Delta\tilde{\boldsymbol{\omega}}\boldsymbol{I}_s\boldsymbol{\omega} \end{aligned} \tag{13}$$

Therefore, the measured kinematic and dynamic models are summarized as follows:

$$\begin{cases} \dot{\hat{\boldsymbol{q}}}_e = E\left(\hat{\boldsymbol{q}}_e\right)\hat{\boldsymbol{\omega}} + \boldsymbol{\delta}_1 \\ \hat{\boldsymbol{J}}\dot{\hat{\boldsymbol{\omega}}} + \tilde{\hat{\boldsymbol{\omega}}}\hat{\boldsymbol{I}}_s\hat{\boldsymbol{\omega}} = \boldsymbol{\delta}_2 + \boldsymbol{u} \end{cases} \tag{14}$$

D. DESIGN OBJECTIVE

The desired attitude $\boldsymbol{q}_{ev}$ and $\boldsymbol{\omega}$ are set as $\boldsymbol{q}_{ev} = [0\ 0\ 0]^{\mathrm{T}}$, and $\boldsymbol{\omega} = [0\ 0\ 0]^{\mathrm{T}}$ in this paper. The subsequent work is to design a robust controller for the system (14) such that, for any initial attitude quaternion and angular velocity:

1) all the state vectors in the closed-loop system are bounded;
2) the measured attitude parameter $\hat{\boldsymbol{q}}_{ev}$ and $\hat{\boldsymbol{\omega}}$ converge to origin asymptotically, and the actual $\boldsymbol{q}_{ev}$, $\boldsymbol{\omega}$ converge to small neighbourhoods of origin simultaneously in the presences of measurment errors, parametric uncertainties and external disturbance.

Remark 1: When $\boldsymbol{q}_{ev} = [0\ 0\ 0]^{\mathrm{T}}$, it yields $q_{e0} = \pm 1$ according to the normalization of quaternion. It should be pointed out that the equilibrium $\boldsymbol{q}_e = [1\ 0\ 0\ 0]^{\mathrm{T}}$ and $\boldsymbol{q}_e = [-1\ 0\ 0\ 0]^{\mathrm{T}}$ indicate the same stable state in physical space. Therefore, it is applicable to force the vector part $\boldsymbol{q}_{ev}$ to origin in the control design.

III. DISTURBANCE-OBSERVER-BASED CONTROLLER DESIGN

A disturbance-observer-based attitude controller is proposed for the rigid-flexible coupling spacecraft in this section. The structure for the anti-disturbance control strategy is illustrated in Fig.3.

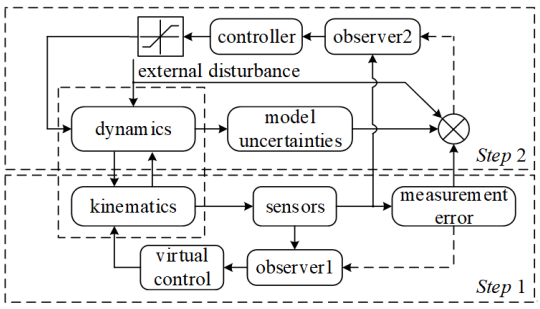

FIGURE 3. Schematic diagram of the control strategy.

The attitude control scheme is developed via the backstepping method. Corresponding to the measured kinematic and dynamic equations(14), the anti-disturbance backstepping controller is constructed in two steps.

Step 1: Define the backstepping variables as:

$$\begin{cases} \boldsymbol{z}_1 = \hat{\boldsymbol{q}}_e \\ \boldsymbol{z}_2 = \hat{\boldsymbol{\omega}} - \boldsymbol{\alpha} \end{cases} \tag{15}$$

where $\boldsymbol{\alpha} \in \mathbb{R}^{3\times 1}$ is the virtual control vector, and it is designed as:

$$\boldsymbol{\alpha} = -E^{-1}(\boldsymbol{z}_1)\left(\boldsymbol{K}_1\boldsymbol{z}_1 + \hat{\boldsymbol{\delta}}_1\right), \tag{16}$$

$E^{-1}(\boldsymbol{z}_1)$ is the generalized inverse matrix of $E(\boldsymbol{z}_1)$, $\boldsymbol{K}_1 \in \mathbb{R}^{4\times 4}$ is a positive definite diagonal matrix, $\hat{\boldsymbol{\delta}}_1$ is the estimation of the lumped disturbances $\boldsymbol{\delta}_1$, and it can be obtained by the FTISMDO [31]:

$$\boldsymbol{s}_0 = \hat{\boldsymbol{q}}_e - \boldsymbol{\psi} \tag{17}$$

$$\dot{\boldsymbol{\psi}} = E(\hat{\boldsymbol{q}}_e)\hat{\boldsymbol{\omega}} + \hat{\boldsymbol{\delta}}_1 \tag{18}$$

$$\boldsymbol{s}_{1j} = \dot{\boldsymbol{s}}_{0j} + \int_0^t \left(k_{1j}\mathrm{sig}^{\beta_{1j}}(\boldsymbol{s}_{0j}) + k_{2j}\mathrm{sig}^{\beta_{2j}}(\dot{\boldsymbol{s}}_{0j})\right)\mathrm{ds} \tag{19}$$

$$\begin{aligned}\dot{\hat{\boldsymbol{\delta}}}_1 = {} & k_{1j}\mathrm{sig}^{\beta_{1j}}(\boldsymbol{s}_{0j}) + k_{2j}\mathrm{sig}^{\beta_{2j}}(\dot{\boldsymbol{s}}_{0j}) + \lambda_{1j}\mathrm{sig}^{\gamma}(\boldsymbol{s}_{1j}) \\ & + \lambda_{2j}\boldsymbol{s}_{1j} + L_j\mathrm{sgn}\left(\boldsymbol{s}_{1j}\right).\end{aligned} \tag{20}$$

In (20), $\boldsymbol{s}_0 = [s_{01}\ s_{02}\ s_{03}\ s_{04}]^{\mathrm{T}}, j = 1, 2, 3, 4.\ k_{1j}, k_{2j}, \beta_{1j}, \beta_{2j}$, λ_{1j}, λ_{2j}, L_j and γ are positive constants. $L_j \geq \sup_{t\geq 0}\left\|\dot{\boldsymbol{\delta}}_1\right\|$, and $\beta_{2j} = \beta_{1j}/\left(1+\beta_{1j}\right)$, $0 < \beta_{1j} < 1$. $\mathrm{sig}^{\beta_{1j}}\left(s_{0j}\right) = \left|s_{oj}\right|^{\beta_{1j}}\mathrm{sgn}\left(s_{0j}\right)$, where $\mathrm{sgn}(\cdot)$ means the sign function, the similar way goes for $\mathrm{sig}^{\beta_{2j}}\left(\dot{s}_{oj}\right)$ and $\mathrm{sig}^{\gamma}\left(s_1\right)$.

The integral term in (17) guarantees the finite time convergence performance of the sliding mode observer. In addition, according to (20), the estimated $\hat{\boldsymbol{\delta}}_1$ is derived by an integral operation which can effectively attenuate the chattering effect. The stability proof for the error system based on observer (17)-(20) is similar to [31], and it is omitted here for space reason.

Remark 2: It can be seen that $\dot{\boldsymbol{s}}_{0i}$ are required to be used in the observer. In this design, the higher-order sliding mode differentiator (HOSMD) [44] is utilized to solve this problem, which is as follows:

$$\begin{aligned}
\dot{\boldsymbol{x}}_0 &= \boldsymbol{v}_0 = -\eta_k|\boldsymbol{x}_0 - f(t)|^{k/(k+1)}\mathrm{sgn}\left(\boldsymbol{x}_0 - f(t)\right) + \boldsymbol{x}_1 \\
\dot{\boldsymbol{x}}_1 &= \boldsymbol{v}_1 = -\eta_{k-1}|\boldsymbol{x}_1 - \boldsymbol{v}_0|^{(k-1)/k}\mathrm{sgn}\left(\boldsymbol{x}_1 - \boldsymbol{v}_0\right) + \boldsymbol{x}_2 \\
&\vdots \\
\dot{\boldsymbol{x}}_{k-1} &= \boldsymbol{v}_{k-1} \\
&= -\eta_1|\boldsymbol{x}_{k-1} - \boldsymbol{v}_{k-2}|^{1/2}\mathrm{sgn}\left(\boldsymbol{x}_{k-1} - \boldsymbol{v}_{k-2}\right) + \boldsymbol{x}_k \\
\dot{\boldsymbol{x}}_k &= -\eta_0\mathrm{sgn}\left(\boldsymbol{x}_1 - \boldsymbol{v}_0\right)
\end{aligned} \tag{21}$$

where $\eta_0, \eta_1, \cdots, \eta_k > 0$ are properly chosen positive constants. The following equalities hold after a finite-time transient process:

$$\begin{cases} \boldsymbol{x}_0 = f_0(t) \\ \boldsymbol{x}_r = \boldsymbol{v}_{r-1} = f_0^{(r-1)}(t), \quad r = 1, 2, \cdots, r \end{cases} \tag{22}$$

For the aforementioned FTISMDO, the $f(t)$ indicates $\boldsymbol{s}_{oi}$, and $\dot{\boldsymbol{s}}_{oi}$ can be obtained by $\boldsymbol{v}_1$.

Remark 3: The FTISMDO requires the upper bound of $\dot{\boldsymbol{\delta}}_1$, $\dot{\hat{\boldsymbol{q}}}_e$ and $\dot{\hat{\boldsymbol{\omega}}}$. Here, $\dot{\boldsymbol{\delta}}_1$ contains the information of $\Delta\dot{\boldsymbol{q}}_e$ and $\Delta\dot{\boldsymbol{\omega}}$, whose bounds are known as $\Delta\bar{\dot{\boldsymbol{q}}}_e$ and $\Delta\bar{\dot{\boldsymbol{\omega}}}$ respectively. Meanwhile, $\dot{\hat{\boldsymbol{q}}}_e$ can be obtained from $\hat{\boldsymbol{q}}_e$ and $\hat{\boldsymbol{\omega}}$, and $\dot{\hat{\boldsymbol{\omega}}}$ can be calculated by the finite-difference method [45] from $\hat{\boldsymbol{\omega}}$. Hence, the upper bound of $\dot{\hat{\boldsymbol{\delta}}}_1$ can be properly obtained.

Step 2: The measured dynamic equation in terms of backstepping variables can be written as:

$$\hat{\boldsymbol{J}}\left(\dot{\boldsymbol{z}}_2 + \dot{\boldsymbol{\alpha}}\right) + \left(\tilde{\boldsymbol{z}}_2 + \tilde{\boldsymbol{\alpha}}\right)\hat{\boldsymbol{I}}_s\left(\boldsymbol{z}_2 + \boldsymbol{\alpha}\right) = \boldsymbol{\delta}_2 + \boldsymbol{u} \tag{23}$$

where $\tilde{\boldsymbol{z}}_2$ and $\tilde{\boldsymbol{\alpha}}$ represents the skew symmetric matrix of $\boldsymbol{z}_2$ and $\boldsymbol{\alpha}$ respectively. Therefore, $\dot{\boldsymbol{z}}_2$ can be expressed as:

$$\dot{\boldsymbol{z}}_2 = -\hat{\boldsymbol{J}}^{-1}\left[\left(\tilde{\boldsymbol{z}}_2 + \tilde{\boldsymbol{\alpha}}\right)\hat{\boldsymbol{I}}_s\left(\boldsymbol{z}_2 + \boldsymbol{\alpha}\right)\right] + \hat{\boldsymbol{J}}^{-1}\boldsymbol{u} + \boldsymbol{\delta}_3 \tag{24}$$

where $\boldsymbol{\delta}_3$ is the lumped uncertainties and is described as follows:

$$\boldsymbol{\delta}_3 = -\dot{\boldsymbol{\alpha}} + \hat{\boldsymbol{J}}^{-1}\boldsymbol{\delta}_2 \tag{25}$$

The control law $\boldsymbol{u}$ is designed as:

$$\boldsymbol{u} = -\hat{\boldsymbol{J}}\boldsymbol{K}_2 z_2 - \hat{\boldsymbol{J}}\hat{\boldsymbol{\delta}}_3 + (\tilde{z}_2 + \tilde{\boldsymbol{\alpha}})\,\hat{\boldsymbol{I}}_s\,(z_2 + \boldsymbol{\alpha}) - \varepsilon\hat{\boldsymbol{J}}\,(E\,(z_1))^{\mathrm{T}} z_1 \tag{26}$$

where $\boldsymbol{K}_2 \in \mathbb{R}^{3\times 3}$ is a positive definite diagonal matrix, ε is a positive constant, and satisfies $0 < \varepsilon \leq 1$, $\hat{\boldsymbol{\delta}}_3$ is the estimation of $\boldsymbol{\delta}_3$ which is obtained by FTISMDO.

Remark 4: The FTISMDO for $\boldsymbol{\delta}_3$ can be described as:

$$\boldsymbol{l}_0 = z_2 - \boldsymbol{\varsigma} \tag{27}$$

$$\dot{\boldsymbol{\varsigma}} = -\hat{\boldsymbol{J}}^{-1}\left[(\tilde{z}_2 + \tilde{\boldsymbol{\alpha}})\,\hat{\boldsymbol{I}}_s\,(z_2 + \boldsymbol{\alpha})\right] + \hat{\boldsymbol{J}}^{-1}\boldsymbol{u} + \hat{\boldsymbol{\delta}}_3 \tag{28}$$

$$\boldsymbol{l}_{1n} = \dot{\boldsymbol{l}}_{0n} + \int_0^t \left(p_{1n}\mathrm{sig}^{\phi_{1n}}(\boldsymbol{l}_{0n}) + p_{2n}\mathrm{sig}^{\phi_{2n}}(\dot{\boldsymbol{l}}_{0n})\right)\mathrm{ds} \tag{29}$$

$$\dot{\hat{\boldsymbol{\delta}}}_3 = p_{1n}\mathrm{sig}^{\phi_{1n}}(\boldsymbol{l}_{0n}) + p_{2n}\mathrm{sig}^{\phi_{2n}}(\dot{\boldsymbol{l}}_{0n}) + \vartheta_{1n}\mathrm{sig}^{\nu}(\boldsymbol{l}_{1n}) + \vartheta_{2n}\boldsymbol{l}_{1n} + L'_n\mathrm{sgn}\,(\boldsymbol{l}_{1n}) \tag{30}$$

where $\boldsymbol{l}_0 = [l_{01} \quad l_{02} \quad l_{03}]^{\mathrm{T}}$, $n = 1, 2, 3$. p_{1n}, p_{2n}, ϕ_{1n}, ϕ_{2n}, ϑ_{1n}, ϑ_{2n}, L'_n and ν are positive constants, $L'_j \geq \sup_{t\geq 0}\left\|\dot{\boldsymbol{\delta}}_3\right\|$, and $\phi_{2p} = \phi_{1p}/\left(1 + \phi_{1p}\right)$, $0 < \phi_{1p} < 1$.

Remark 5: The upper bound of $\dot{\boldsymbol{\delta}}_3$ is requried for L'_j. Similar to *Remark* 3, bounds of $\Delta\dot{\bar{\boldsymbol{q}}}_e$, $\Delta\dot{\bar{\boldsymbol{\omega}}}$, $\dot{\hat{\boldsymbol{q}}}_e$ and $\dot{\hat{\boldsymbol{\omega}}}$ are available. According to (11), $4\boldsymbol{F}_{sa}\boldsymbol{\xi}_a\boldsymbol{\Omega}_a\dot{\boldsymbol{\eta}}_a + 2\boldsymbol{F}_{sa}\boldsymbol{\Lambda}_a\boldsymbol{\eta}_a$ is equivalent to $\boldsymbol{u} + \boldsymbol{d} - \boldsymbol{J}\left(\dot{\hat{\boldsymbol{\omega}}} + \Delta\dot{\boldsymbol{\omega}}\right) - \left(\tilde{\hat{\boldsymbol{\omega}}} + \Delta\tilde{\boldsymbol{\omega}}\right)\boldsymbol{I}_s\left(\hat{\boldsymbol{\omega}} + \Delta\boldsymbol{\omega}\right)$, where $\bar{\boldsymbol{d}}$ is available, $\ddot{\bar{\boldsymbol{\omega}}}$ and $\dot{\boldsymbol{u}}$ can be calculated by the finite-difference method [45]. Therefore, the upper bound of $\dot{\boldsymbol{\delta}}_3$ can be properly chosen.

Theorem 1: If the diagonal elements of $\boldsymbol{K}_1$ and $\boldsymbol{K}_2$ satisfy $\boldsymbol{K}_{1d} \geq 1/2\,(d = 1, 2, 3, 4)$ and $\boldsymbol{K}_{2f} \geq 1/2\,(f = 1, 2, 3)$ respectively, then the designed control law $\boldsymbol{u}$ can guarantee that all variables in the closed-loop are bounded, and the controlled states $\boldsymbol{q}_e$ and $\boldsymbol{\omega}$ converge to origin in finite time.

Proof: The candidate Lyapunov function V_1 is defined as:

$$V_1 = \frac{1}{2}{z_1}^{\mathrm{T}} z_1 \tag{31}$$

Based on $\boldsymbol{\alpha}$(16) and $\hat{\boldsymbol{\delta}}_1$(20), the derivative of V_1 is derived as:

$$\begin{aligned}\dot{V}_1 &= {z_1}^{\mathrm{T}}\dot{z}_1 \\ &= {z_1}^{\mathrm{T}}\left(E\,(z_1)\,(z_2 + \boldsymbol{\alpha}) + \boldsymbol{\delta}_1\right) \\ &= -{z_1}^{\mathrm{T}}\boldsymbol{K}_1 z_1 + {z_1}^{\mathrm{T}}\tilde{\boldsymbol{\delta}}_1\end{aligned} \tag{32}$$

where $\tilde{\boldsymbol{\delta}}_1 = \boldsymbol{\delta}_1 - \hat{\boldsymbol{\delta}}_1$ is the estimation error of $\hat{\boldsymbol{\delta}}_1$.

Further, the second candidate Lyapunov function is proposed as:

$$V_2 = \frac{1}{2}{z_2}^{\mathrm{T}} z_2 + \varepsilon V_1 \tag{33}$$

Set $\tilde{\boldsymbol{\delta}}_3$ as the estimation error of $\hat{\boldsymbol{\delta}}_3$, and $\tilde{\boldsymbol{\delta}}_3 = \boldsymbol{\delta}_3 - \hat{\boldsymbol{\delta}}_3$ holds. Based on (24),(26),(32), the time derivative of V_2 is derived as follows:

$$\begin{aligned}\dot{V}_2 &= {z_2}^{\mathrm{T}}\dot{z}_2 + \varepsilon\dot{V}_1 \\ &= {z_2}^{\mathrm{T}}\left(-\hat{\boldsymbol{J}}^{-1}\left[(\tilde{z}_2 + \tilde{\boldsymbol{\alpha}})\,\hat{\boldsymbol{I}}_s\,(z_2 + \boldsymbol{\alpha})\right] + \boldsymbol{\delta}_3 + \hat{\boldsymbol{J}}^{-1}\boldsymbol{u}\right) \\ &\quad + \varepsilon\left(-{z_1}^{\mathrm{T}}\boldsymbol{K}_1 z_1 + {z_1}^{\mathrm{T}}\tilde{\boldsymbol{\delta}}_1\right) \\ &= {z_2}^{\mathrm{T}}\left(-\boldsymbol{K}_2 z_2 + \boldsymbol{\delta}_3 - \hat{\boldsymbol{\delta}}_3\right) - \varepsilon{z_1}^{\mathrm{T}}\boldsymbol{K}_1 z_1 + \varepsilon{z_1}^{\mathrm{T}}\tilde{\boldsymbol{\delta}}_1 \\ &= -\varepsilon{z_1}^{\mathrm{T}}\boldsymbol{K}_1 z_1 - {z_2}^{\mathrm{T}}\boldsymbol{K}_2 z_2 + \varepsilon{z_1}^{\mathrm{T}}\tilde{\boldsymbol{\delta}}_1 + {z_2}^{\mathrm{T}}\tilde{\boldsymbol{\delta}}_3 \\ &\leq -\varepsilon{z_1}^{\mathrm{T}}\boldsymbol{K}_1 z_1 - {z_2}^{\mathrm{T}}\boldsymbol{K}_2 z_2 + \frac{1}{2}\varepsilon\left({z_1}^{\mathrm{T}} z_1 + \tilde{\boldsymbol{\delta}}_1^{\mathrm{T}}\tilde{\boldsymbol{\delta}}_1\right) \\ &\quad + \frac{1}{2}\left({z_2}^{\mathrm{T}} z_2 + \tilde{\boldsymbol{\delta}}_3^{\mathrm{T}}\tilde{\boldsymbol{\delta}}_3\right) \\ &= -\varepsilon{z_1}^{\mathrm{T}}\left(\boldsymbol{K}_1 - \frac{1}{2}\boldsymbol{I}_4\right)z_1 - {z_2}^{\mathrm{T}}\left(\boldsymbol{K}_2 - \frac{1}{2}\boldsymbol{I}_3\right)z_2 \\ &\quad + \frac{1}{2}\left(\varepsilon\tilde{\boldsymbol{\delta}}_1^{\mathrm{T}}\tilde{\boldsymbol{\delta}}_1 + \tilde{\boldsymbol{\delta}}_3^{\mathrm{T}}\tilde{\boldsymbol{\delta}}_3\right)\end{aligned} \tag{34}$$

According the finite-time convergence of the FTISMDO, the estimation errors $\tilde{\boldsymbol{\delta}}_1$ and $\tilde{\boldsymbol{\delta}}_3$ would converge to zero after a finite time t_f. In addition, the diagonal elements of $\boldsymbol{K}_1$ and $\boldsymbol{K}_2$ guarantee that $(\boldsymbol{K}_1 - 1/2\boldsymbol{I}_4)$ and $(\boldsymbol{K}_2 - 1/2\boldsymbol{I}_3)$ are positive definite matrices. Therefore, after t_f, $\dot{V}_2$ can be transformed as:

$$\dot{V}_2 \leq -\varepsilon{z_1}^{\mathrm{T}}\left(\boldsymbol{K}_1 - \frac{1}{2}\boldsymbol{I}_4\right)z_1 - {z_2}^{\mathrm{T}}\left(\boldsymbol{K}_2 - \frac{1}{2}\boldsymbol{I}_3\right)z_2 \leq 0 \tag{35}$$

As a result, we prove that the attitude control system under the proposed controller is asymptotically stable, and the states z_1 and z_2 will converge to origin asymptotically. As $\hat{\boldsymbol{q}}_e \to 0$ and $\hat{\boldsymbol{\omega}} \to 0$, the actual attitude parameters $\boldsymbol{q}_e$ and $\boldsymbol{\omega}$ will converge to small neighbourhoods of origin respectively. In addition, it can be concluded from (35) that V_2 decreases from a bounded initial value $V_2(0)$ to zero. Therefore, all the states in the closed-loop are bounded under the anti-disturbance attitude controller.

IV. NUMERICAL EXAMPLE

In this section, we will present a simulation example to illustrate the effectiveness of the proposed technique. The performance of the attitude controller is verified on a rigid satellite with two symmetric solar arrays.

The spacecraft mass inertial nominal component is given as: $\hat{\boldsymbol{I}}_s = [57\ 9\ 12;\ 9\ 51\ 6;\ 12\ 6\ 57]\mathrm{kg}\cdot\mathrm{m}^2$, and its uncertain component is: $\Delta\boldsymbol{I}_s = [0.06\ 0.05\ 0.01;\ 0.03\ 0.07\ 0.002;\ 0.02\ 0.001\ 0.09]\mathrm{kg}\cdot\mathrm{m}^2$. The flexible coupling coefficient matrix for each of the solar array's vibration to the spacecraft's rotation is:

$$\boldsymbol{F}_{sa} = \begin{bmatrix} 1.4015 & -1.1673 & 2.1987 & 1.2018 \\ 1.2807 & 1.0201 & 1.5673 & -1.5782 \\ 2.1397 & -1.2653 & -0.7967 & 1.2304 \end{bmatrix}$$

The modal frequency and damping diagonal matrix of each solar array is: $\boldsymbol{\Omega}_a = \mathrm{diag}\,\{1.5908, 2.2757, 1.9482, 2.4858\}$,

$\boldsymbol{\xi}_a = \text{diag}\{0.1133, 0.1712, 0.1548, 0.0578\}$. Hence, $\boldsymbol{\Lambda}_a = \text{diag}\{2.5308, 5.1789, 3.7953, 6.1794\}$.

The external disturbance is defined as: $\boldsymbol{d} = 0.02[1 + \sin(0.013\pi t),\ 1 + \sin(0.012\pi t),\ 1 + \sin(0.010\pi t)]^{\mathrm{T}}$. In addition, the measurement errors include: $\Delta\boldsymbol{q}_e = 0.002[1 + \sin(0.023\pi t),\ 1 + \sin(0.023\pi t), 1 + \sin(0.021\pi t), 1 + \sin(0.013\pi t)]^{\mathrm{T}}$, $\Delta\boldsymbol{\omega} = 0.002[1 + \sin(0.023\pi t),\ 1 + \sin(0.021\pi t), 1 + \sin(0.013\pi t)]^{\mathrm{T}}$.

The initial quaternion, angular velocity and modal coordinate are given as: $\boldsymbol{q}_e(0) = [0.173648,\ -0.263201,\ 0.789603,\ -0.526402]^{\mathrm{T}}$, $\boldsymbol{\omega}(0) = [10^\circ,\ -9^\circ,\ 13^\circ]^{\mathrm{T}}$, $\boldsymbol{\eta}_a(0) = \mathbf{0}$, $\dot{\boldsymbol{\eta}}_a = \mathbf{0}$. The gains for controller are described as:

$\boldsymbol{K}_1 = \text{diag}\{65.62, 66.18, 65.99, 66.13\}$, $\boldsymbol{K}_2 = \text{diag}\{65.99,\ 65.90,\ 65.93\}$.

The observer gains are given as: for $\hat{\boldsymbol{\delta}}_1$, $k_{11} = 0.24\text{e-}5$, $k_{12} = 0.21\text{e-}5$, $k_{13} = 0.23\text{e-}5$, $k_{14} = 0.22\text{e-}5$, $k_{21} = 0.31\text{e-}5$, $k_{22} = 0.28\text{e-}5$, $k_{23} = 0.27\text{e-}5$, $k_{24} = 0.29\text{e-}5$, $\lambda_{11} = 1.65\text{e-}5$, $\lambda_{12} = 1.83\text{e-}5$, $\lambda_{13} = 1.85\text{e-}5$, $\lambda_{14} = 1.77\text{e-}5$, $\lambda_{21} = 1.62\text{e-}5$, $\lambda_{22} = 1.65\text{e-}5$, $\lambda_{23} = 1.59\text{e-}5$, $\lambda_{24} = 1.63\text{e-}5$, $\gamma = 4.89\text{e-}3$, $\beta_{11} = 0.0020$, $\beta_{12} = 0.0019$, $\beta_{13} = 0.0023$, $\beta_{14} = 0.0021$, $L_1 = 0.859\text{e-}5$, $L_2 = 0.895\text{e-}5$, $L_3 = 0.860\text{e-}5$, $L_4 = 0.905\text{e-}5$. For $\hat{\boldsymbol{\delta}}_3$, $p_{11} = 5.12\text{e-}2$, $p_{12} = 5.29\text{e-}2$, $p_{13} = 5.30\text{e-}2$, $p_{21} = 6.30\text{e-}2$, $p_{22} = 6.25\text{e-}2$, $p_{23} = 6.28\text{e-}2$, $\vartheta_{11} = 1.3\text{e-}2$, $\vartheta_{12} = 1.1\text{e-}2$, $\vartheta_{13} = 1.2\text{e-}2$, $\vartheta_{21} = 1.0\text{e-}2$, $\vartheta_{22} = 1.9\text{e-}2$, $\vartheta_{23} = 1.2\text{e-}2$, $\nu = 0.89$, $\phi_{11} = 0.36$, $\phi_{12} = 0.36$, $\phi_{13} = 0.36$, $L_1' = 3.9\text{e-}5$, $L_2' = 3.9\text{e-}5$, $L_3' = 3.9\text{e-}5$, $L_4' = 3.9\text{e-}5$.

The HOSMD Gains for both $\hat{\boldsymbol{\delta}}_1$ and $\hat{\boldsymbol{\delta}}_3$ are given as $\eta_0 = 0.15$, $\eta_1 = 2.5$, $\eta_2 = 6.5$, $\eta_3 = 2.5$, $\eta_4 = 13.8$.

The simulation results are presented in Fig.4-Fig.11. Fig.4-Fig.5 illustrates the trajectory of the measured and actual quaternion respectively.

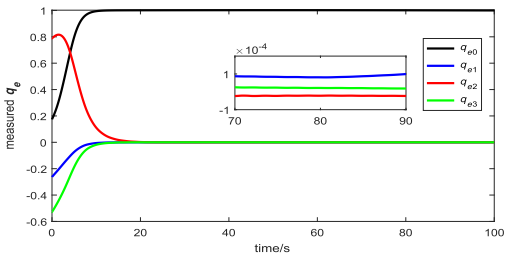

FIGURE 4. Trajectory of the measured quaternion.

From Fig.4 it can be seen that the measured quaternion converges to origin asymptotically, while the convergence error of the actual quaternion is larger, which is caused by the measurement error in the model. The trajectory of the measured and actual angular velocity are presented in Fig.6-Fig.7 respectively.

Similar with $\hat{\boldsymbol{q}}_e$ and $\boldsymbol{q}_e$, the convergence error of $\boldsymbol{\omega}$ in Fig.7 is also larger than that of $\hat{\boldsymbol{\omega}}$ in Fig.6. The development of the solar array's modal coordinate is given in Fig.8.

It can be observed from Fig.8 that all of the modal coordinates($N = 4$) converge to small neighborhood of origin gradually, while the convergence speed is slower than

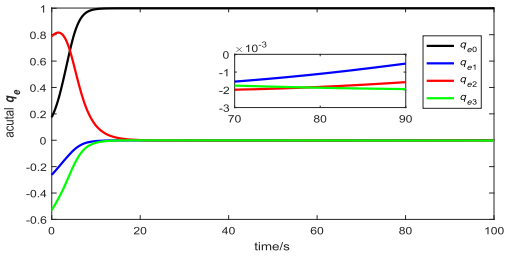

FIGURE 5. Trajectory of the actual quaternion.

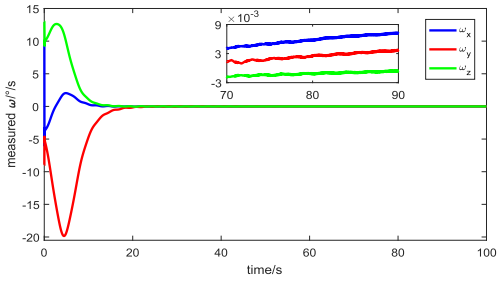

FIGURE 6. Trajectory of the measured attitude angular.

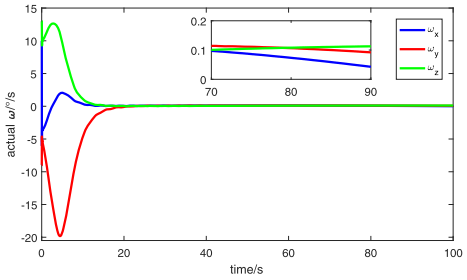

FIGURE 7. Trajectory of the actual attitude angular.

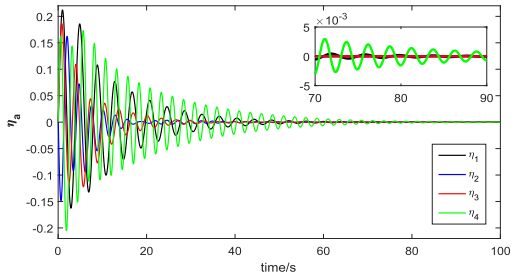

FIGURE 8. Trajectory of the modal coordinate.

that of the attitude states in Fig.4-Fig.7. The reason is that the attitude states converging to origin means the gradual vanishment of the vibration exicitement, while the flexible appendages require more time to calm down.

Fig.4-Fig.8 verify the effectiveness of the proposed controller in the presence of various disturbances. With ± 1Nm being the control input constraint, the trajectory of the proposed controller is illustrated in Fig.9.

The actual lumped uncertainties $\boldsymbol{\delta}_1$ and its estimation $\hat{\boldsymbol{\delta}}_1$, and $\boldsymbol{\delta}_3$ and its estimation $\hat{\boldsymbol{\delta}}_3$ are respectively presented

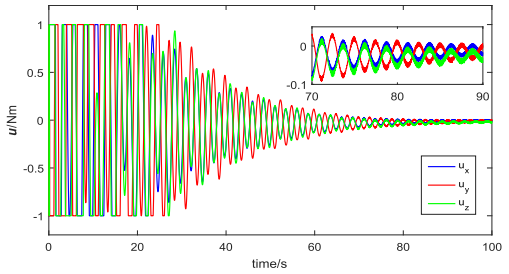

FIGURE 9. Trajectory of the control torque.

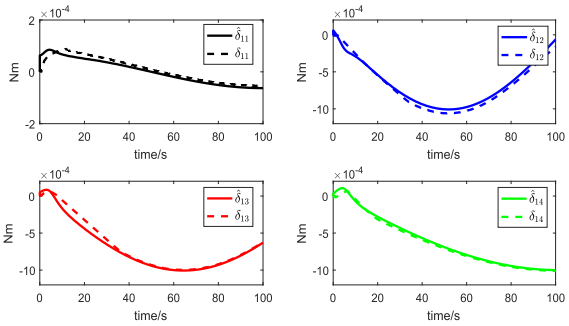

FIGURE 10. δ_1 and its estimation $\hat{\delta}_1$.

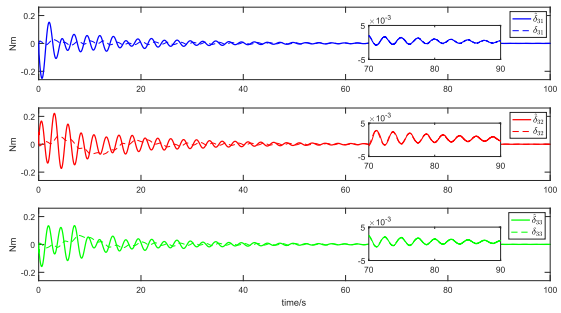

FIGURE 11. δ_3 and its estimation $\hat{\delta}_3$.

in Fig.10-Fig.11. The subfigures indicate each of the vector components.

Fig.10-Fig.11 illustrates that the two observers can effectively evaluate the lumped disturbances during the controlling process.

V. CONCLUSION

In this paper, an anti-disturbance backstepping control scheme has been proposed for the attitude stabilization of the rigid-flexible coupling spacecraft. The robust controller is structured in two steps via the backstepping method. With the inertia uncertainties, external disturbance and measurement errors being considered, the FTISMDO is utilized twice in the controller design process to estimate lumped uncertainties. The simulation results verify that the FTISMDO-based backstepping controller is robust to various disturbances, and can effectively solve the attitude stabilization problem for rigid-flexible coupling spacecraft.

REFERENCES

[1] Q. Hu, X. Shao, and W.-H. Chen, "Robust fault-tolerant tracking control for spacecraft proximity operations using time-varying sliding mode," *IEEE Trans. Aerosp. Electron. Syst.*, vol. 54, no. 1, p. 2–17, Feb. 2018.

[2] L. Sun, W. Huo, and Z. Jiao, "Adaptive backstepping control of spacecraft rendezvous and proximity operations with input saturation and full-state constraint," *IEEE Trans. Ind. Electron.*, vol. 64, no. 1, pp. 480–492, Jan. 2017.

[3] A. Weiss, M. Baldwin, R. S. Erwin, and I. Kolmanovsky, "Model predictive control for spacecraft rendezvous and docking: Strategies for handling constraints and case studies," *IEEE Trans. Control Syst. Technol.*, vol. 23, no. 4, pp. 1638–1647, Jul. 2015.

[4] H. Peng and X. Bai, "Natural deep space satellite constellation in the earth-moon elliptic system," *Acta Astronautica*, Jan. 2018.

[5] B. Shahbazi, M. Malekzadeh, and H. R. Koofigar, "Robust constrained attitude control of spacecraft formation flying in the presence of disturbances," *IEEE Trans. Aerosp. Electron. Syst.*, vol. 55, no. 5, pp. 2534–2543, Oct. 2017.

[6] S. Eshghi and R. Varatharajoo, "Nonsingular terminal sliding mode control technique for attitude tracking problem of a small satellite with combined energy and attitude control system (CEACS)," *Aerosp. Sci. Technol.*, vol. 76, pp. 14–26, May 2018.

[7] L. Sun and Z. Zheng, "Disturbance-observer-based robust backstepping attitude stabilization of spacecraft under input saturation and measurement uncertainty," *IEEE Trans. Ind. Electron.*, vol. 64, no. 10, pp. 7994–8002, Oct. 2017.

[8] S. Di Gennaro, "Active vibration suppression for flexible spacecraft," in *Proc. Eur. Control Conf.*, Jul. 1997, pp. 3590–3595.

[9] J. Wang and D. Li, "Experiments study on attitude coupling control method for flexible spacecraft," *Acta Astronautica*, vol. 147, pp. 393–402, Jun. 2018.

[10] J. Yang, W.-H. Chen, and Z. Ding, "Disturbance observers and applications," *Trans. Inst. Meas. Control*, vol. 38, no. 6, pp. 621–624, 2016.

[11] K. Ohishi, M. Nakao, K. Ohnishi, and K. Miyachi, "Microprocessor-controlled DC motor for load-insensitive position servo system," *IEEE Trans. Ind. Electron.*, vol. IE-34, no. 1, pp. 44–49, Feb. 1987.

[12] S. Kwon and W. K. Chung, "A discrete-time design and analysis of perturbation observer for motion control applications," *IEEE Trans. Control Syst. Technol.*, vol. 11, no. 3, pp. 399–407, May 2003.

[13] H. Jingqing, "The 'extended state observer' of a class of uncertain systems," *Control Decision*, vol. 10, no. 1, PP. 85–87, 1995.

[14] C. Johnson, "Optimal control of the linear regulator with constant disturbances," *IEEE Trans. Autom. Control*, vol. 13, no. 4, pp. 416–421, Aug. 1968.

[15] W.-H. Chen, J. Yang, L. Guo, and S. Li, "Disturbance-observer-based control and related methods—An overview," *IEEE Trans. Ind. Electron.*, vol. 63, no. 2, pp. 1083–1095, Feb. 2016.

[16] D. Lee, "Nonlinear disturbance observer-based robust control for spacecraft formation flying," *Aerosp. Sci. Technol.*, vol. 76, pp. 82–90, May 2018.

[17] H. Wang, W. Liu, J. Qiu, and P. X. Liu, "Adaptive fuzzy decentralized control for a class of strong interconnected nonlinear systems with unmodeled dynamics," *IEEE Trans. Fuzzy Syst.*, vol. 26, no. 2, pp. 836–846, Apr. 2018.

[18] L. Zhang, Y. Zhu, and W. X. Zheng, "State estimation of discrete-time switched neural networks with multiple communication channels," *IEEE Trans. Cybern.*, vol. 47, no. 4, pp. 1028–1040, Apr. 2017.

[19] X. Zhao, L. Zhang, P. Shi, and M. Liu, "Stability and stabilization of switched linear systems with mode-dependent average dwell time," *IEEE Trans. Autom. Control*, vol. 57, no. 7, pp. 1809–1815, Jul. 2012.

[20] X. Zhao, P. Shi, and X. Zheng, "Fuzzy adaptive control design and discretization for a class of nonlinear uncertain systems," *IEEE Trans. Cybern.*, vol. 46, no. 6, pp. 1476–1483, Jun. 2016.

[21] Y. Zhu, Z. Zhong, W. X. Zheng, and D. Zhou, "HMM-Based $H\infty$ filtering for discrete-time Markov jump LPV systems over unreliable communication channels," *IEEE Trans. Syst., Man, Cybern., Syst.*, to be published.

[22] S. Feng and H.-N. Wu, "Hybrid robust boundary and fuzzy control for disturbance attenuation of nonlinear coupled ODE-beam systems with application to a flexible spacecraft," *IEEE Trans. Fuzzy Syst.*, vol. 25, no. 5, pp. 1293–1305, Oct. 2017.

[23] L. Wu, P. Shi, and H. Gao, "State estimation and sliding-mode control of Markovian jump singular systems," *IEEE Trans. Autom. Control*, vol. 55, no. 5, pp. 1213–1219, May 2010.

[24] H. Li, Z. Feng, X. Li, L. Liu, and B. Niu, "Decentralized adaptive approximation-based fuzzy output-feedback control of uncertain switched stochastic interconnected nonlinear systems," *J. Franklin Inst.*, vol. 354, no. 16, pp. 7306–7325, 2017.
[25] X. Zhao, Y. Yin, B. Niu, and X. Zheng, "Stabilization for a class of switched nonlinear systems with novel average dwell time switching by T–S fuzzy modeling," *IEEE Trans. Cybern.*, vol. 46, no. 8, pp. 1952–1957, Aug. 2016.
[26] X. Zhao, X. Wang, G. Zong, and H. Li, "Fuzzy-approximation-based adaptive output-feedback control for uncertain non-smooth nonlinear systems," *IEEE Trans. Fuzzy Syst.*, to be published.
[27] F. Gao, X. Hu, S. E. Li, K. Li, and Q. Sun, "Distributed adaptive sliding mode control of vehicular platoon with uncertain interaction topology," *IEEE Trans. Ind. Electron.*, vol. 68, no. 8, pp. 6352–6361, Aug. 2018.
[28] M. Liu, P. Shi, L. Zhang, and X. Zhao, "Fault-tolerant control for nonlinear Markovian jump systems via proportional and derivative sliding mode observer technique," *IEEE Trans. Circuits Syst. I, Reg. Papers*, vol. 58, no. 11, pp. 2755–2764, Nov. 2011.
[29] P. Zhang, J. Qiao, L. Guo, and W. Li, "Sliding mode friction observer based control for flexible spacecraft with reaction wheel," *IET Control Theory Appl.*, vol. 11, no. 8, pp. 1274–1281, May 2017.
[30] M. Chen, Q.-X. Wu, and R.-X. Cui, "Terminal sliding mode tracking control for a class of SISO uncertain nonlinear systems," *ISA Trans.*, vol. 52, no. 2, pp. 198–210, 2013.
[31] H. Sun, L. Hou, G. Zong, and L. Guo, "Composite anti-disturbance attitude and vibration control for flexible spacecraft," *IET Theory Appl.*, vol. 11, no. 14, pp. 2383–2390, Sep. 2017.
[32] A. A. Bolonkin and N. S. Khot, "Optimal bounded control design for vibration suppression," *Acta Astronautica*, vol. 38, no. 10, pp. 803–813, 1996.
[33] E. Azadi, M. Eghtesad, S. A. Fazelzadeh, and M. Azadi, "Vibration suppression of smart nonlinear flexible appendages of a rotating satellite by using hybrid adaptive sliding mode/Lyapunov control," *J. Vib. Control*, vol. 19, no. 7, pp. 975–991, 2013.
[34] X. Zhao, P. Shi, Y. Yin, and S. K. Nguang, "New results on stability of slowly switched systems: A multiple discontinuous Lyapunov function approach," *IEEE Trans. Autom. Control*, vol. 62, no. 7, pp. 3502–3509, Jul. 2017.
[35] J. Wang, Y. Gao, J. Qiu, and C. K. Ahn, "Sliding mode control for non-linear systems by Takagi–Sugeno fuzzy model and delta operator approaches," *IET Control Theory Appl.*, vol. 11, no. 8, pp. 1205–1213, May 2017.
[36] Y. Ma, B. Jiang, G. Tao, and Y. Cheng, "Uncertainty decomposition-based fault-tolerant adaptive control of flexible spacecraft," *IEEE Trans. Aerosp. Electron. Syst.*, vol. 51, no. 2, pp. 1053–1068, Apr. 2015.
[37] X. Zhao, X. Wang, G. Zong, and X. Zheng, "Adaptive neural tracking control for switched high-order stochastic nonlinear systems," *IEEE Trans. Cybern.*, vol. 47, no. 10, pp. 3088–3099, Oct. 2017.
[38] Y. Lv, Z. Wang, Y. Guo, and L. Chen, "Back-stepping based integrated orbit and attitude control for on-orbit servicing spacecraft," in *Proc. IEEE Chin. Guid., Navigat. Control Conf.*, Aug. 2017, pp. 2325–2330.
[39] H. Wang, P. X. Liu, S. Li, and D. Wang, "Adaptive neural output-feedback control for a class of nonlower triangular nonlinear systems with unmodeled dynamics," *IEEE Trans. Neural Netw. Learn. Syst.*, vol. 29, no. 8, pp. 3658–3668, Aug. 2018.
[40] S. Ding and W. X. Zheng, "Nonsmooth attitude stabilization of a flexible spacecraft," *IEEE Trans. Aerosp. Electron. Syst.*, vol. 50, no. 2, pp. 1163–1181, Apr. 2014.
[41] S. Wu and S. Wen, "Robust $H\infty$ output feedback control for attitude stabilization of a flexible spacecraft," *Nonlinear Dyn.*, vol. 84, no. 1, pp. 405–412, 2016.
[42] H. Du and S. Li, "Attitude synchronization for flexible spacecraft with communication delays," *IEEE Trans. Autom. Control*, vol. AC-61, no. 11, pp. 3625–3630, Nov. 2016.
[43] M. Bingqi, Q. Guangji, X. Suiqin, and C. Daosheng, "Lagrange's equations in quasicoordinates for dynamics modeling of flexible spacecraft," *Chin. Space Sci. Technol.*, vol. 23, no. 2, pp. 1–6, Apr. 2003.
[44] J. E. Stott and Y. B. Shtessel, "Launch vehicle attitude control using sliding mode control and observation techniques," *J. Franklin Inst.*, vol. 349, no. 2, pp. 397–412, 2012.
[45] H. O. Walther, "Book review: Introduction to functional differential equations," *Bull. Amer. Math. Soc.*, vol. 32, no. 1, pp. 132–137, 1995.

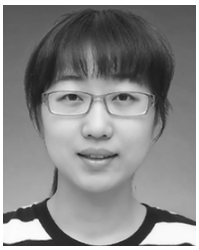

YUE MIAO received the B.S. degree in spacecraft design and engineering and the M.S. degree in aerospace science and technology from the Harbin Institute of Technology, Harbin, China, in 2014 and 2016 respectively, where she is currently pursuing the Ph.D. degree in aerospace science and technology.

Her research interests include spacecraft attitude robust control and autonomous task planning for formation flying satellites.

FENG WANG received the first Ph.D. degree in aerospace science and technology from the Harbin Institute of Technology, Harbin, China in 2008, and the second Ph.D. degree from Cranfield University, U.K., in 2010. Since 2014, he has been a Professor with the School of Astronautics, Harbin Institute of Technology.

His research fields include dynamics and control of distributed satellites systems, on orbit service for spacecraft, general design of nanosatellites, and spacecraft attitude control.

MING LIU received the B.S. and M.S. degrees in formation and computing science and in operational research and cybernetics from Northeastern University, Liaoning, China, in 2003 and 2006 respectively, and the Ph.D. degree in mathematics from the City University of Hong Kong in 2009. Since 2015, he has been a Professor with the School of Astronautics, Harbin Institute of Technology.

His research interests include networked control systems, quantized control systems, fault estimation, fault-tolerant control, and robust control/filtering.